Applied Catalysis B: Environmental 89 (2009) 494–502

Contents lists available at ScienceDirect

Applied Catalysis B: Environmental

journal homepage: www.elsevier.com/locate/apcatb

Effect of TiO_2 particle size on the photocatalytic reduction of CO_2

K. Kočí [a,*], L. Obalová [a], L. Matějová [b], D. Plachá [a], Z. Lacný [a], J. Jirkovský [c], O. Šolcová [b]

[a] Technical University of Ostrava, 17. listopadu 15, Ostrava, Czech Republic
[b] Institute of Chemical Process Fundamentals CAS, Rozvojová 135, Prague, Czech Republic
[c] J. Heyrovsky Institute of Physical Chemistry CAS, Dolejškova 3, Prague, Czech Republic

ARTICLE INFO

Article history:
Received 1 October 2008
Received in revised form 15 January 2009
Accepted 18 January 2009
Available online 24 January 2009

Keywords:
CO_2 reduction
TiO_2
Photocatalysis
Size effect

ABSTRACT

Pure TiO_2 anatase particles with a crystallite diameters ranging from 4.5 to 29 nm were prepared by precipitation and sol–gel method, characterized by X-ray diffraction (XRD), BET surface area measurement, UV–vis and scanning electron microscopy (SEM) and tested in CO_2 photocatalytic reduction. Methane and methanol were the main reduction products. The optimum particle size corresponding to the highest yields of both products was 14 nm. The observed optimum particle size is a result of competing effects of specific surface area, charge–carrier dynamics and light absorption efficiency.

1. Introduction

Carbon dioxide (CO_2) is the main contributor to the greenhouse effect. The global concentration of CO_2 in the atmosphere is increasing mainly due to the emissions from fossil fuel combustion. The reduction of CO_2 by photocatalysts is one of the most promising methods since CO_2 can be reduced to useful compounds by irradiating it with UV light at room temperature and ambient pressure.

Several semiconductors exhibit band gap energies suitable for the photocatalytic reduction of carbon dioxide (for example ZnS [1], CdS [1–4], ZrO_2 [5–10], MgO [11,12] and ZnO [13]). These catalysts are suitable for the title reaction because their conduction band energy (Ecb) is adequately negative compared to the reduction potentials of CO_2. However, among the applied photocatalysts, TiO_2 is one of the most widely employed photocatalytic semiconducting materials [14–41], although its conduction band energy is comparable to the reduction potentials of CO_2 (e.g., the latter is −0.24 V for reduction of CO_2 toward CH_4). From a thermodynamic point of view, an efficient photocatalyst should have a more negative Ecb compared to the reduction potentials of CO_2 [42]. The main reasons are the peculiarities of chemical inertness, non-photocorrosion, low cost, stability against photoirradiation and non-toxicity [43].

The rate of the photocatalytic reaction can be controlled by several steps: light absorption, transport of photogenerated charges (electron e^- and hole h^+) onto the photocatalyst surface, recombination of e^- and h^+, reaction of e^- and h^+ on the photocatalyst surface and mass transfer of reactants to the catalyst surface. The surface morphology of a photocatalyst, namely the particle size and agglomerate size, is a very important parameter influencing the aforementioned steps.

A good photocatalyst must have high photon conversion efficiency in addition to the high specific surface area. In fact, the primary particle size of the photocatalyst determines both the specific surface area and the photon conversion efficiency. However, the relationship between the particle size and photocatalytic reactivity for CO_2 reduction has not been clarified yet and only a few studies have dealt with this topic.

Zhang et al. [44] showed that particle size plays an important role in nanocrystalline TiO_2 based catalysts mostly by influencing the dynamics of e^-/h^+ recombination. Particle size of about 10 nm might be the optimal value for a pure TiO_2 photocatalyst in liquid phase decomposition of $CHCl_3$.

Xu et al. [45] and Jang et al. [46] have experimentally studied the effect of TiO_2 particle size on the photocatalytic degradation of methylene blue (MB) in a suspended aqueous solution. The results suggested that the adsorption rate and adsorbed amount of MB on suspended TiO_2 particles increased while the TiO_2 particle size decreased. The photocatalytic activity of TiO_2 also increased while the TiO_2 particle size was reduced, especially when the particle size was less than 30 nm.

Maira et al. [47] studied the photocatalytic degradation of trichloroethylene (TCE) in gas phase upon TiO_2 in the size range of 2.3 and 27 nm. They reported an optimum particle size of 7 nm. For TiO_2 catalysts with primary particles or crystal size larger than

* Corresponding author. Tel.: +420 596991592.
E-mail address: kamila.koci@vsb.cz (K. Kočí).

0926-3373/$ – see front matter © 2009 Elsevier B.V. All rights reserved.
doi:10.1016/j.apcatb.2009.01.010

7 nm the following dependency is valid; smaller crystals offer a larger surface area and exhibit a higher TCE degradation, while TiO_2 catalysts with a primary particle size smaller than 7 nm show a larger surface area but a lower TCE degradation.

Hao et al. [48] reported an increase in photodegradation of rhodanide B with a decrease of particle sizes (150, 16 and 8 nm). They explained it by the fact that the organic substrate is strongly adsorbed and thus the direct charge transfer is the rate-determining step.

Almquist and Biswas [49] compared the effect of particle size using TiO_2 prepared with sizes ranging from 5 to 165 nm, commercial TiO_2 Degussa P25 and Aldrich anatase. The results of photooxidation of organic substrates in water elucidated a strong particle size effect on photoactivity; the optimal particle size ranged from 25 to 40 nm.

Another issue related to the effect of particle size on the photocatalytic reaction is the primary vs. the secondary particle size. Primary particle is an aggregate of microcrystals where the microcrystals are separated from each other by very fine pores (primary pores). The size of the microcrystals and primary pores depends on the conditions used for the preparation of the catalyst (type of precursors, pH, postsynthesis operations, temperature of thermal treatment, etc.). Secondary particle size is the size of the catalyst grain that resulted from the aggregation of TiO_2 primary particles [50]. The aggregation of primary particles is difficult to avoid and originates due to factors such as charge density/potential of particle surfaces and van der Waals forces. Results of the photocatalytic oxidation of 2-chlorophenol (2-CP) by Lin et al. [51] showed that the smaller the particle size, the faster the degradation rate. Results also showed that the secondary particle size grew with time mainly due to particle aggregation. The photocatalytic rate constants decreased exponentially with the increase of the primary particle size. The primary particle size alone is able to predict the photocatalytic rate as it is closely related to the electro-optical properties of photocatalysts.

Krýsa et al. [52] showed that Q particles (size 3–4 nm) forming agglomerates (1–2 μm) exhibit only a slightly lower photoactivity than P25 (size 15 nm) in 0.15 μm agglomerates. Comparing these results with 10 times lower photoactivity of non-agglomerated Q-TiO_2 particles in relation to P25 [53], they concluded that the agglomerisation of particles plays an important role in the photocatalytic degradation rate.

However, all of these studies refer to the photocatalytic oxidation reactions, i.e., reactions which are based on the oxidation potential of photogenerated holes. In this case the CO_2 reduction is based on the reduction potential of photogenerated electrons and the dependence of photocatalytic performance on particle size has not been done yet.

The band gap of the semiconductor becomes larger with decreasing particle size, i.e., valence band energy (Evb) is moderately shifted to lower energies and Ecb is strongly shifted to higher energies [54]. This is one of the reasons why it is generally possible to control photocatalytic performance by varying the size of the semiconductor particles.

The aim of this work is to assess the effect of the primary particle size on the photocatalytic reactivity of TiO_2 exemplified by the photoreduction of CO_2 by water. The photocatalytic reduction of CO_2 in our experimental arrangement runs in liquid phase with suspended TiO_2. However, the reduction products are analyzed in both phases (liquid and gas), which can only be found rarely in literature [16,21,25,36].

The experimental conditions for the CO_2 photocatalytic reduction were set according to the knowledge found in scientific literature [25,31,36]. Although water acts as the reducing agent in the photocatalytic reduction of CO_2, NaOH water solution is often used in this reaction. There are two reasons for it: (i) an increase of dissolved CO_2 amount because the caustic NaOH solution dissolves more CO_2 than pure water, (ii) reduction of the recombination of hole–electron pairs leading to a longer decay time of surface electrons and facilitation of CO_2 reduction because the highly-concentrated OH^- ions in aqueous solution could act as strong hole-scavengers and form $^{\bullet}OH$ radicals. The optimum concentration of NaOH was reported to be 0.2 M [25,31] and this concentration is also applied in this work.

The concentration of suspended TiO_2 catalyst in a photocatalytic reaction should be below 1 g/dm^3 to avoid a light-scattering effect caused by a high TiO_2 concentration and prevent hindering the light's ability to reach every catalyst particle [31,36]. In all our experiments, a catalyst concentration of 1 g/dm^3 was applied.

2. Experimental

2.1. TiO_2 preparation

Pure TiO_2 anatase particles with crystallite diameters ranging from 4.5 to 29 nm were prepared by (1) precipitation method using titanium(IV) alkoxide and a dilute solution of hydrogen peroxide and by (2) sol–gel method controlled in an inverse micellar environment of Triton X-114 (see Fig. 1) in cyclohexane.

(1) 20 ml of titanium(IV) n-butoxide (Aldrich, purity >98+%) was slowly added into 50 ml of ice-cooled 4.4 M H_2O_2 solution (30% p.a., Lach-Ner). During the 30 min experiment at 0 °C, the formation of an orange $Ti{\cdot}H_2O_2$ complex was observed together with oxygen, water and alcohol. Before filtration, the prepared precipitate was exposed to air for one day and then dried at 105 °C for 24 h. During drying the orange precipitate converted into a white precipitate. After drying, the precipitate was calcinated at above 250 °C for 4 h to guarantee a Ti–O–O– bond creation and alcohol decomposition. Samples were calcinated at 300 and 400 °C.

(2) The TiO_2 powder was prepared by mixing cyclohexane (Aldrich, purity >99%), Triton X-114 (Aldrich), distilled water and titanium(IV) n-butoxide (Aldrich, purity >98+%) in a molar ratio of $11C_6H_{12}{:}1C_{29}H_{52}O_{8.5}{:}1H_2O{:}1Ti(OCH(CH_3)_2)_4$ (volume ratio $C_{29}H_{52}O_{8.5}/C_6H_{12} = 0.49$) at ambient temperature and pressure. The titanium gel was obtained after one day of aging in the air. The gel was calcinated at 400 °C with a temperature ramp 1 °C/min in air stream for 4 h.

The prepared TiO_2 samples were denoted according to their particle size determined by X-ray diffraction (XRD) and methods of preparation. The preparation conditions, crystallite size and denotation of prepared TiO_2 samples are summarized in Table 1.

2.2. Characterization of TiO_2 catalysts

The TiO_2 powders were characterized by various techniques to specify their structural and textural properties; crystalline phase and crystallite size by X-ray diffraction, specific surface area by nitrogen physical adsorption at 77 K, absorption properties by UV–vis absorbance and morphology by scanning electron microscopy (SEM).

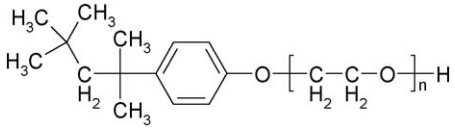

Fig. 1. Non-ionic surfactant Triton X. In case Triton X-114 the number of oxyethylene units is $n = 7$. Summary formula: $C_{29}H_{52}O_{8.5}$, Physical properties: Mol. weight = 558.8 g/mol, density = 1.058 g/cm^3.

Table 1
Preparation conditions, crystallite size of prepared TiO_2 samples.

Catalyst	Preparation method	Titanium precursor	H_2O_2 concentration (%)	Calcination conditions (°C/h)	Crystallite size[a] (nm)
4.5A-1	1[b]	n-Butoxide	15	300/4	4.5 ± 0.8
4.5B-1	1	n-Butoxide	25	300/4	4.5 ± 0.8
6-2	2[c]	Isopropoxide	–	400/4	6 ± 2
8-1	1	n-Butoxide	15	380/4	8.1 ± 1
14-1	1	Isopropoxide	15	400/4	14 ± 1
29-1	1	Isopropoxide	15	400/10	29 ± 1

[a] Evaluated by modified FOX program by fitting X-ray diffraction patterns.
[b] Precipitation method.
[c] Sol–gel method.

The XRD measurements of all samples were performed using the Seifert-FMP or the Panalytical-MPD laboratory diffractometer with a Cu anode in the conventionally focused Bragg-Brentano experimental arrangement in the measured range of $2\Theta = 10$–105°. The diameter of the anatase crystallites was evaluated by a modified FOX program (developed at Faculty of Mathematics and Physics, Charles University in Prague [55]) designed for microstructure determination from powder diffraction patterns (FOX = - Free Objects for Crystallography [56]).

The surface area and porous structure of the prepared catalysts were determined by adsorption/desorption of nitrogen at −196 °C using ASAP 2010 instrument (Micromeritics, USA) and evaluated by the BET and BJH methods, respectively. Prior to the adsorption measurement, all samples were degassed at 110 °C until a pressure level of 0.1 Pa was attained (~12 h).

Energy band gap of the synthesized materials was determined spectroscopically. The diffuse reflectance spectra of the power photocatalysts placed in a 5 mm quartz cell were measured using the Lambda 19 UV/VIS/NIR spectrophotometer (PerkinElmer) equipped with an integrating sphere. The original coordinates of the spectra (reflectance vs. wavelength) were transformed to Kubelka-Munk function (K) vs. photon energy ($h\nu$) [57–59]. The final plots of $(Kh\nu)^{1/2}$ as a function of $h\nu$ are in accordance with the theoretical equation [60–62],

$$h\nu\alpha = \text{const}(h\nu - E_{bg})^2 \quad (1)$$

where α is the absorption coefficient of the photocatalyst and E_{bg} the energy band gap. (The Kubelka-Munk function K calculated from the reflectance spectra [63] is predetermined to be directly proportional to the absorption coefficient α.) The values of the energy band gap are usually estimated by extrapolation of the linear part of the dependence. However, we employed a more precise method based on the fitting of experimental dependences by Boltzmann symmetrical functions by means of non-linear regression. Then the calculated crossing point of the tangent line in the inflection point of the Boltzmann fit with its lower asymptote determines the energy band gap as shown in Fig. 2.

The JEOL JSM-5500LV scanning electron microscope was used for the study of the TiO_2 particles morphology.

The organic elemental analysis performed on the Elementar vario EL III (Elementar Comp.) was used for purity determination of the prepared titania samples. In all cases the carbon content was under 0.1% – the detection limit of the analysis.

2.3. Photocatalytic reactivity experiments

The photocatalytic reduction of carbon dioxide was carried out in a homemade apparatus (Fig. 3).

A stirred batch annular reactor (length 35 cm, width 3.5 cm) with a suspended catalyst was illuminated by an 8 W Hg lamp with a peak light intensity at 254 nm (Ultra-Violet Products Inc., USA, 11SC-1) situated in the center of the quartz tube; the shell tube was made from stainless steel. The internal volume was 380 cm^3. The catalyst powder (0.1 g) was suspended in 100 ml of 0.2 M NaOH solutions for typical batches. Supercritical fluid-grade CO_2 with a certified maximum of hydrocarbons less than 1 ppm was used as the reactant (SIAD Technical Gases, CZ) to avoid any hydrocarbon contamination. A magnetic stirrer at the bottom agitated the catalyst-suspended solution to prevent sedimentation of the catalyst. The temperature and pH of the solution and the pressure of the gas phase were continuously monitored.

Prior to the illumination, CO_2 was bubbled with a constant flow through the stirred suspension for at least 30 min to purge the air and to saturate the solution. The reactor was tightly closed and the CO_2 pressure was maintained at 110 kPa. Then the photocatalytic reaction was started by switching on the Hg lamp.

Samples of gas and liquid reaction mixture were taken at various times during the irradiation. Small aliquots of the suspension were withdrawn by a syringe, filtered through a Millipore filter membrane and analyzed. Gas sampling was performed using a gas-tight syringe (10 ml) through a septum and the samples were immediately analyzed.

An UVC probe was attached to the outer wall of the quartz tube with the same diameter as the stainless steel shell tube and the energy flux (mW/cm^2) was indicated by a lumen meter connected to the probe. The photon flux was obtained by dividing the energy flux by the energy of a photon with a wavelength of 254 nm. The energy flux was first measured for the reactor filled with water only (1.72 mW/cm^2). It was then measured for the reactor containing the catalyst and CO_2 during the reaction (0.31 mW/cm^2). The difference between those energy fluxes was the photo energy absorbed during the CO_2 photoreduction (1.41 mW/cm^2).

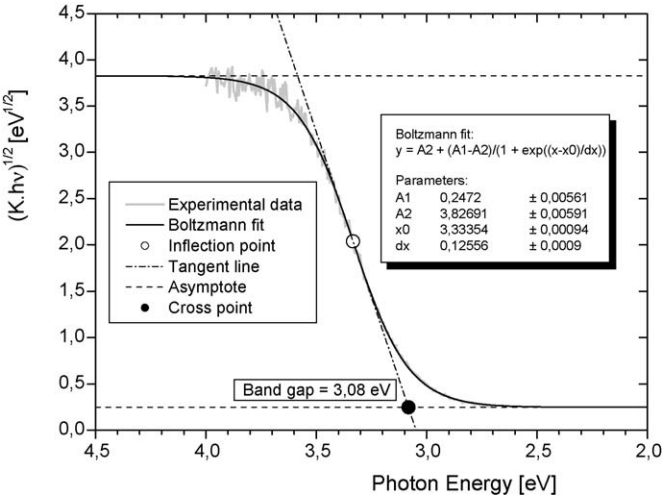

Fig. 2. Determination of energy band gap from a transformed diffuse reflectance spectrum (see text for details).

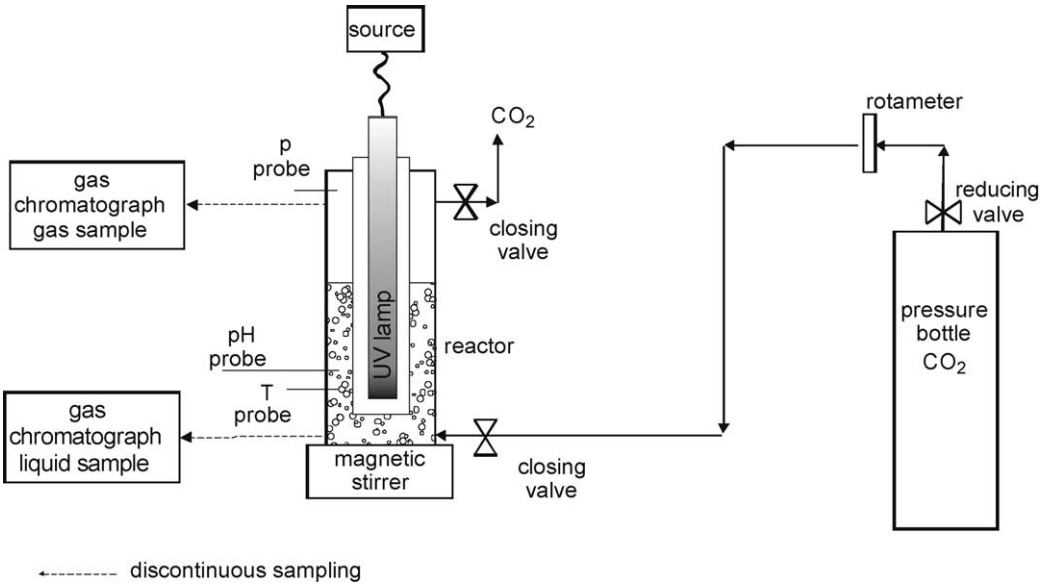

Fig. 3. Block scheme of the apparatus for CO_2 photocatalytic reduction.

Blank reactions were performed to ensure that the hydrocarbon production was due to the photoreduction of CO_2 and to eliminate the surrounding interference. The first blank was UV-illuminated without the catalyst, the second was in the dark with the catalyst and CO_2 under the same experimental conditions and the third was over the illuminated photocatalyst in the absence of CO_2. No hydrocarbons were detected in the above blank tests.

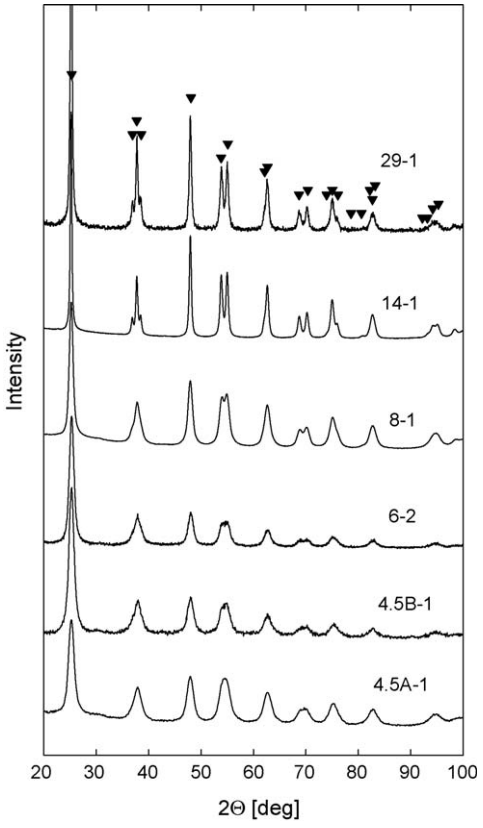

Fig. 4. XRD patterns of TiO_2 powders. (▼) anatase.

2.4. Analyses of CO_2 photoreduction products

The gas phase samples were analyzed using a gas chromatograph (GC-Agilent Technologies 6890N) equipped with FID and TCD detectors and the Molsieve and HP Poraplot Q columns for methane, hydrogen, ethane, carbon monoxide, carbon dioxide, oxygen and nitrogen analysis. The calibration with certified calibration gases (1.5 mol% CH_4, 0.987 mol% H_2, 0.0493 mol% C_2H_6, 2.02 mol% CO, and 99.999 mol% CO_2) was performed before each experimental run.

The samples of the liquid phase were analyzed by a gas chromatograph (GC-Agilent Technologies 6890N) equipped with FID detector and the HP 5 column for methanol and ethanol analysis. A five-point calibration using standard samples was performed. Helium was used as a carrier gas in the case of both GCs.

The modified method for colorimetric formaldehyde determination by chromotropic acid was used [64]. Sample aliquots were reacted with chromotropic acid in the presence of sulfuric acid to form a purple monocationic chromogen. A Hatch DR 900 spectrophotometer was used for all absorbance measurements. The five-point calibration was done by plotting absorbance against formaldehyde concentration for each calibration level.

3. Results and discussion

3.1. Characterization of TiO_2 nanoparticles

The crystallite size together with the evaluation error was determined by fitting the XRD lines. The results are summarized in Table 1. The XRD patterns of prepared TiO_2 samples are shown in Fig. 4. The structural and basic optical characterizations of tested titania are summarized in Table 2. For samples prepared according

Table 2
The basic optical and structural characterizations of tested samples.

Catalyst	XRD phase character	TiO_2 polymorph phase	Band gap (eV)
4.5A-1	Crystalline	Anatase	3.11
4.5B-1	Crystalline	Anatase	3.14
6-2	Semi-crystalline	Anatase, amorphous	3.00
8-1	Crystalline	Anatase	3.08
14-1	Crystalline	Anatase	3.08
29-1	Crystalline	Anatase	3.09

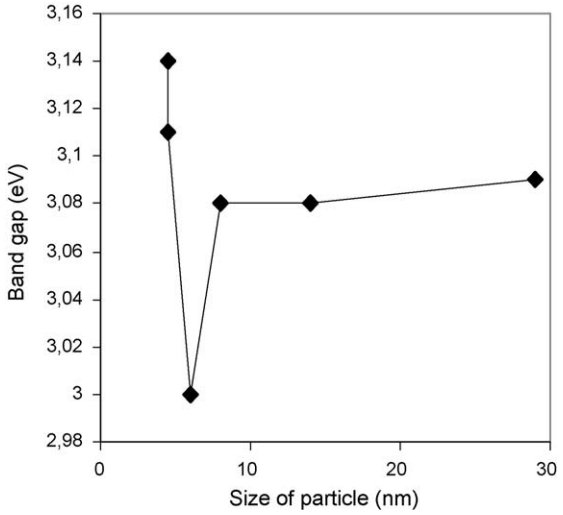

Fig. 5. Band gap of anatase TiO_2 as a function of particle size.

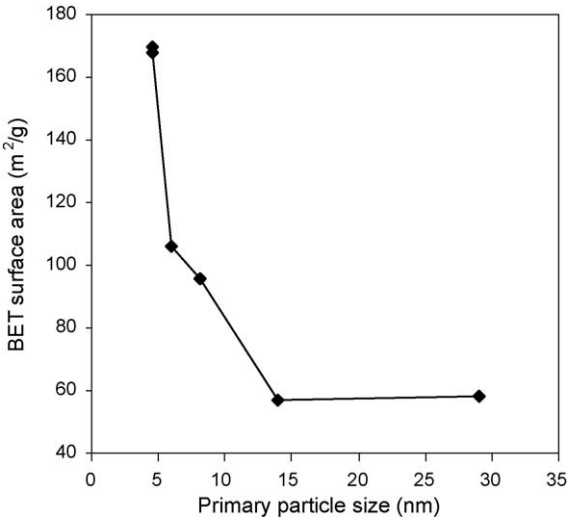

Fig. 6. BET surface area of anatase TiO_2 as a function of particle size.

to Method 1 the pure crystalline anatase phase with a band gap in the range 3.08–3.14 eV is typical. In TiO_2 prepared by sol–gel method, an amorphous background besides the crystalline anatase phase was detected ($2\Theta = 15.64^\circ$ and 19.19°) and the band gap value is the smallest −3 eV. The dependency of the band gap on the particle size is shown in Fig. 5. This dependency corresponds well with the results of Lin et al. [51]. Lin furthermore verified the observed band gap using the Brus's equation, i.e., the effective mass model (EMM) [54,65].

Table 3
The basic textural characteristics of tested samples.

Catalyst	S_{BET} (m^2/g)	S_{meso} (m^2/g)	V_{micro} (mm^3_{liq}/g)	Pore radii (nm)
4.5A-1	170	119	33.9	1.7
4.5B-1	168	122	30.4	1.7
6-2	106	73	22.1	1.8
8-1	96	66	19.8	1.8
14-1	57	38	12.9	1.9
29-1	58	42	13.7	1.7

The basic textural characterizations of the tested samples are summarized in Table 3. The BET surface area of the prepared TiO_2 samples changed significantly with crystallite size, as can be seen in Fig. 6 where the BET surface area of the TiO_2 anatase catalysts as a function of the crystallite sizes is shown.

It is obvious that the catalyst surface area decreases with increasing particle size. The smallest (4.5 nm) and the largest (29 nm) TiO_2 anatase crystals possessed surface areas of 170 and 58 m^2/g, respectively. These results suggest that the catalyst surface area depends only on the size of the TiO_2 anatase crystals. All the prepared TiO_2 samples contained a small volume of micropores. For better imagination of the TiO_2 aggregates, SEM microphotographs of sample 14-1 prepared by hydrolysis of alkoxides in hydrogen peroxide solution (Method 1) are shown in Fig. 7.

3.2. The photocatalytic reduction of CO_2

The effect of irradiation time on the formation of CO_2 photocatalytic reduction products was investigated over a period of 0–24 h on the TiO_2 catalysts with different particle sizes. Fig. 8 shows the evolution of all reaction products as functions of the irradiation for TiO_2 catalyst with a particle size of 14 nm. Two main products were determined: methane in gas phase and methanol in liquid phase. Hydrogen and low amounts of carbon oxide were also detected. Other products such as formic acid, formaldehyde, ethane and ethylene could also be formed [17,36], but they were undetectable in our GC configuration. The observed yields ($\mu mol/g_{cat}$) order was: $H_2 > CH_4 > CH_3OH \geq CO$.

The yields of methane were negligible during the first 5 h of irradiation in all cases (Fig. 9A). A similar trend of yield-time dependency was observed; only the shapes for samples with 4.5 nm particle size (4.5A-1, 4.5B-1) were slightly different. A substantial increase of methane yield was observed after 8 h of irradiation with the exception of the catalyst with 29 nm particle size where a sharp increase was achieved after 15 h. The highest yield of methane was observed for the catalyst with 14 nm particle size (14-1sample).

The yields of methanol were one order of magnitude lower than the yields of methane (Fig. 9B). Data at 5 h were measured but were

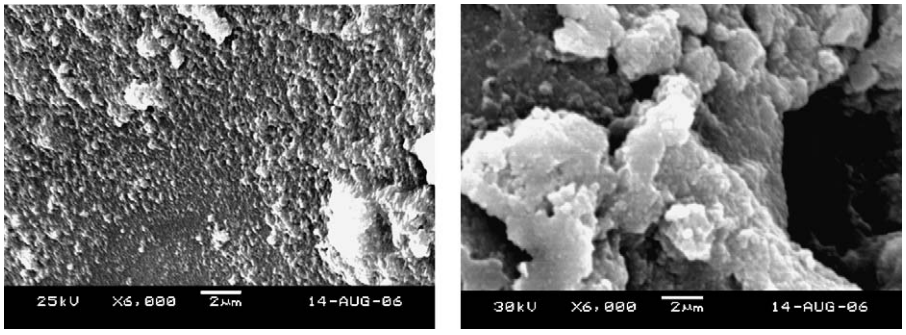

Fig. 7. SEM microphotographs of TiO_2 prepared by hydrolysis of alkoxides in hydrogen peroxide solution – sample 14-1.

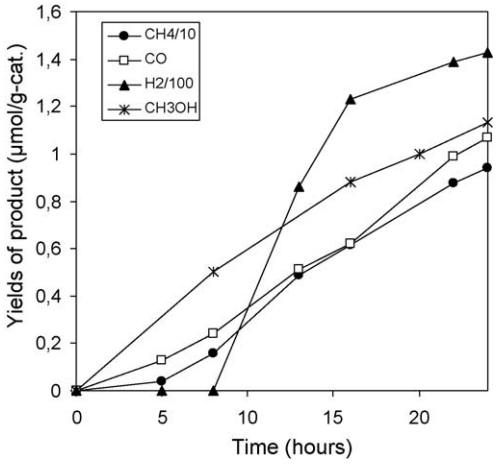

Fig. 8. Time dependence of the product yields over the TiO_2 catalysts with particle size 14 nm.

under the limit of determinableness (12 μg/l, i.e., 0.38 μmol/g_{cat}). The steepest curve of methanol yield was measured for 14-1 TiO_2 catalyst, the most moderate for 4.5A-1 and 4.5B-1 nm.

The hydrogen yields were undeterminable during the first 8 h of irradiation in all cases (Fig. 9C). A rapid increase of hydrogen amount came after 8 h, the deceleration of hydrogen formation was observed after 15 h. The yields of carbon monoxide increased slowly during the reaction but all yields were near the limit of detection (Fig. 9D).

The conversion of CO_2 was calculated from the analyzed amount of CH_4, CH_3OH and CO based on an assumption that the initial molar amount of CO_2 was determined from the gas volume in the reactor at the reaction conditions. The conversion of CO_2 was 0.1%.

The catalyst with the crystallite size of 4.5 nm was prepared twice for verifying the reproducibility of the preparation. Observed physico-chemical properties (Tables 2 and 3) and catalytic measurements (Fig. 9A–D) indicated satisfying results. The results for samples 6-2 and 8-1 suggest the ability to prepare TiO_2 with a predetermined crystallite size by both preparation methods and with good reproducibility of photocatalytic measurements; when the experimental error is taken into account (6 ± 2 and 8 ± 1 nm, respectively) these samples have a similar crystallite size.

Various reaction schemes for the photocatalytic reduction of CO_2 by H_2O on TiO_2 catalysts have been proposed in scientific literature [17,18,25,28,36,37]. The following reforming reactions (2)–(12) would have undergone when the reactants and catalysts are in contact with UV irradiation.

$$TiO_2 \xrightarrow{h\nu} e^-(TiO_2) + h^+(TiO_2) \quad (2)$$

$$e^-(TiO_2) + h^+(TiO_2) \xrightarrow{h\nu} \text{heat} \quad (3)$$

$$4h^+ + 2H_2O_{ads} \xrightarrow{(Ti^{3+}-O^-)^*} O_2 + 4H^+ \quad (4)$$

$$H^+ + e^- \xrightarrow{(Ti^{3+}-O^-)^*} {}^{\bullet}H \quad (5)$$

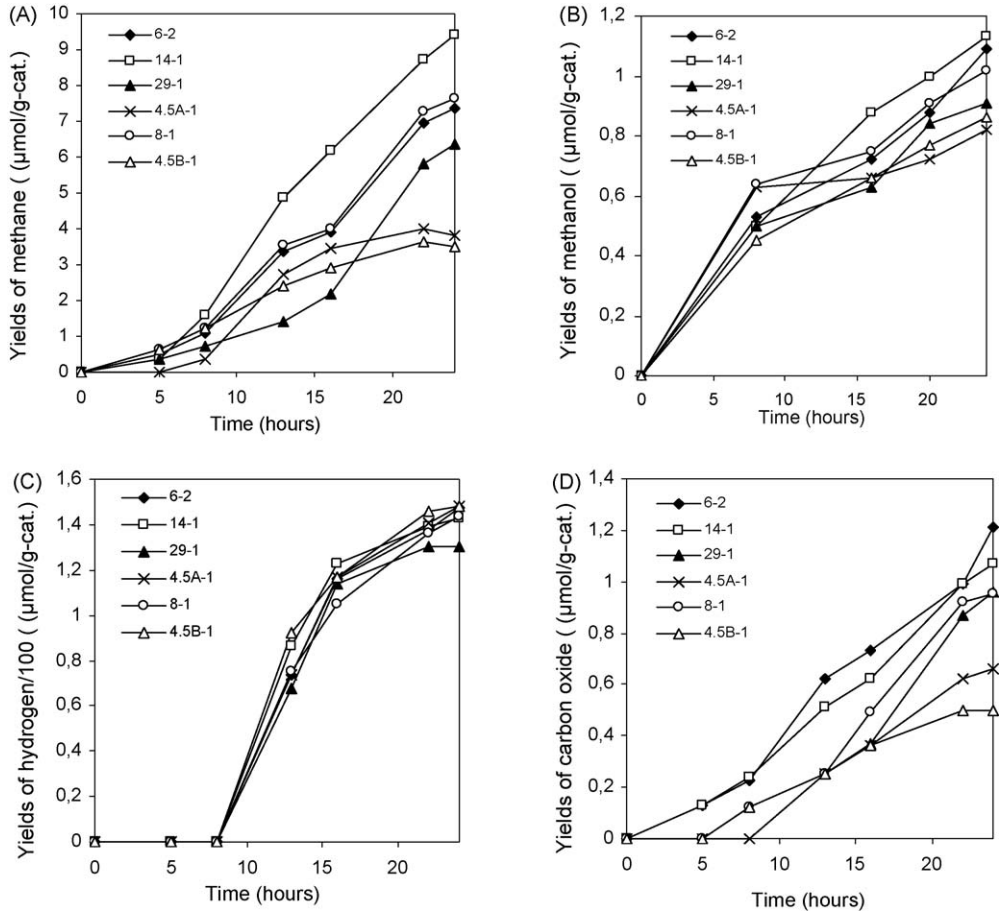

Fig. 9. (A–D) Time dependence of the product yields (A – methane, B – methanol, C – hydrogen, D – carbon monoxide) over the TiO_2 catalysts with different particle size.

$$CO_2 + e^{-} \xrightarrow{(Ti^{3+}-O^-)^*} O-{}^{\bullet}C-O^- \quad (6)$$

$$O-{}^{\bullet}C-O^- + {}^{\bullet}H \xrightarrow{(Ti^{3+}-O^-)^*} CO + OH^- \quad (7)$$

$$CO + e^{-} \xrightarrow{(Ti^{3+}-O^-)^*} {}^{\bullet}CO^- \quad (8)$$

$${}^{\bullet}CO^- + {}^{\bullet}H \xrightarrow{(Ti^{3+}-O^-)^*} C + OH^- \quad (9)$$

$$OH^- + h^+ \xrightarrow{(Ti^{3+}-O^-)^*} OH^{\bullet} \quad (10)$$

$$C + {}^{\bullet}H \xrightarrow{(Ti^{3+}-O^-)^*} {}^{\bullet}CH \quad (11)$$

$${}^{\bullet}CH + {}^{\bullet}H \xrightarrow{(Ti^{3+}-O^-)^*} CH_2 \quad (12)$$

$$CH_2 + {}^{\bullet}H \xrightarrow{(Ti^{3+}-O^-)^*} {}^{\bullet}CH_3 \quad (13)$$

$${}^{\bullet}CH_3 + {}^{\bullet}H \xrightarrow{(Ti^{3+}-O^-)^*} CH_4 \quad (14)$$

$${}^{\bullet}CH_3 + {}^{\bullet}OH \xrightarrow{(Ti^{3+}-O^-)^*} CH_3OH \quad (15)$$

$$2H^{\bullet} \xrightarrow{(Ti^{3+}-O^-)^*} H_2 \quad (16)$$

When illuminated by UV light with a sufficient photonic energy ($h\nu$) and an appropriate wavelength, photon-generated electrons (e^-) and holes (h^+) are created on the surface of the TiO_2 catalysts (Eqs. (2) and (3)). Furthermore, the photoexcited electrons and holes in the lattice are separated and trapped by the appropriate sites of TiO_2 to avoid recombination. The holes first react with water adsorbed on the catalyst, producing oxygen and H^+ (Eq. (4)). The interaction of H^+ ions with the excited electrons leads to the formation of $H^{\bullet}$ radicals (Eq. (5)). At the same time, ${}^{\bullet}CO_2^-$ radicals are formed from CO_2 (Eq. (6)). These incipient ${}^{\bullet}CO_2^-$ and ${}^{\bullet}H$ radicals react with each other to produce CO (Eq. (7)). Then the ${}^{\bullet}CH_3$ radical is formed from CO by consecutive reactions (Eqs. (8)–(13)). The methane is formed by the reaction with the ${}^{\bullet}H$ radical (reaction (14)), while methanol is formed by the reaction with ${}^{\bullet}OH$ (reaction (15)). Hydrogen is formed by the reaction of ${}^{\bullet}H$ radical (Eq. (16)). Generated free oxygen (Eq. (4)) can be partially consumed by re-oxidation of methane. Tan et al. [38] demonstrated that the incipient O_2 could lead to the photooxidation of products back into carbon dioxide in a reverse reaction. Such oxidation process could have affected the reduction process and limited the reduction yields. Incipient methanol can similarly act as a sacrificial agent and in part can be completely oxidated to carbon dioxide and H_2 [66,67].

Pure anatase was identified in all our TiO_2 samples by XRD analysis. Anatase has a tetragonal structure. From a topological standpoint it differs from the other TiO_2 polymorphs by having TiO_6 octahedra which share four edges with other such octahedra [68]. The published results imply that the aggregated octahedrally coordinated titanium oxide species show a high selectivity to produce CH_4 while the highly dispersed titanium tetrahedral Ti-oxide species have a high selectivity for the formation of CH_3OH [22,27]. The observed higher selectivity to methane formation in this work corresponds with active sites comprised by octahedrally coordinated TiO_2 in agreement with the results of XRD analysis.

The effect of the TiO_2 nanocrystalline size on the yields of the two main products related to the weight of the catalyst is depicted in Fig. 10A and B. The best catalyst is the one with a particle size of 14 nm with the exceptions of methane yield in time of 5 h and methanol yield at 8 h due to the high error of GC analysis. The photoreactivity of TiO_2 increases when the particle size is increased from 4.5 to 14 nm, but decreases when it is further increased to 29 nm. Both yields are the highest for a particle size of 14 nm, which might be an optimal value for the TiO_2 photocatalyst in the CO_2 photoreduction. The effect of the primary particle size on the CO_2 photocatalytic reduction has not been studied yet. However, an optimum crystallite size corresponding to the highest yields was found for other photocatalytic reactions which depend on the oxidation potential of photogenerated holes, e.g., the degradation of trichloroethylene (with an optimal crystallite size of 7 nm) [47], phenol (with an optimal crystallite size of 25–40 nm) [49], trichlormethane (with an optimal crystallite size of 10 nm) [44], congo red (with an optimal crystallite size of 10 nm) [69].

Generally, in a photocatalytic slurry system two major factors greatly impact the reaction (a) specific surface area and (b) band gap [51]. The specific surface area determines the available active sites for the reaction to take place. The band gap of the semiconductor catalyst defines the amount of photons that are available for quantum conversion. Data from the longest reaction timespan were chosen for the comparison because yields were the highest and the most accurate. The yields of the two main products expressed per 1 m^2 of catalyst surface (Fig. 11A and B) have similar trends with the highest yields obtained for TiO_2 with a crystallite size of 14 nm (14-1 sample). This indicates that the specific surface area is not the most decisive parameter in the CO_2 photocatalytic reduction and that the observed yield trends of the main products are a result of several factors that overshadow the surface area advantage of ultra-fine particles (less than 14 nm in our case): (i)

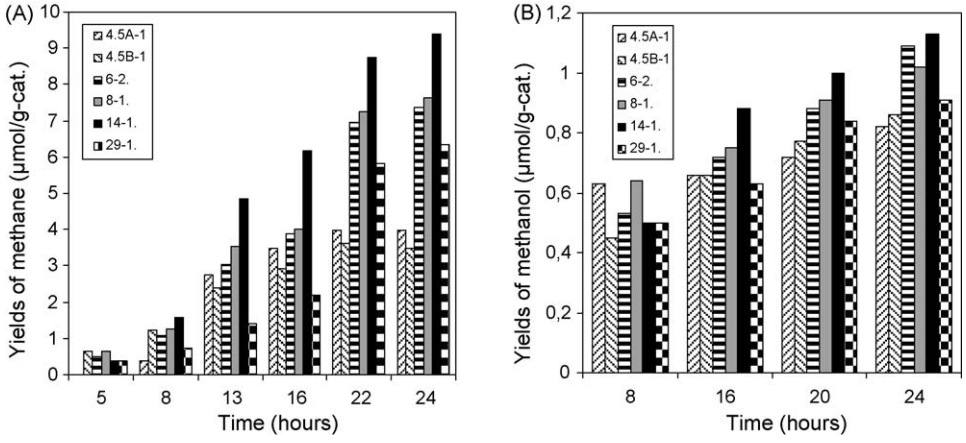

Fig. 10. (A and B) Time dependence of the product yields (A – methane, B – methanol) over the TiO_2 catalysts with different particle size.

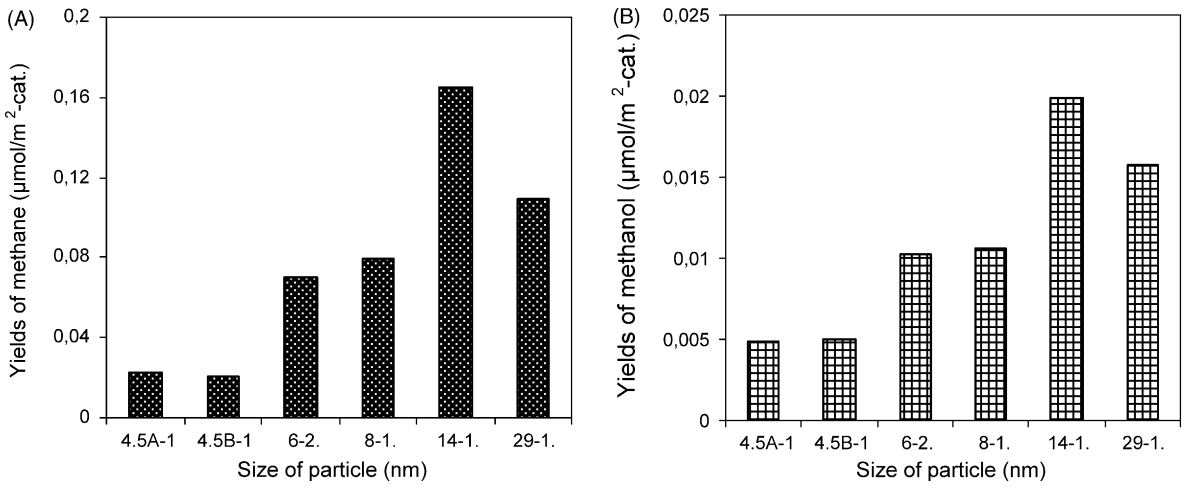

Fig. 11. (A and B) Dependence of the product yields (after 24 h of irradiation) on the particle size.

increase in surface electron–hole recombination, (ii) particle aggregation and (iii) size quantization effect. When the particle size decreases, the density of recombination centers increases, which supports the recombination of holes and electrons [44,51,70]. Ultra-fine particles (<14 nm) can undergo rapid flocculation, which decreases the availability of active surface sites [47,51]. The quantization effect caused a band gap increase as the particle size decreased under a certain minimum value, leading to a decrease of photoactivity. A plausible explanation for this change in band gap with respect to the size of the particle is that the bulk defects induce a delocalization of the molecular orbital in the conduction band edge (e.g., LUMO) and create shallow/deep traps in electronic energy, in turn causing the red-shift of the absorption spectra. When the crystallite size decreased below its size at the band gap minimum, the traps shifted to higher energy, which resulted in blue shifting of the absorption spectra (e.g., size quantization effect) [51,54,65].

4. Conclusion

Photocatalytic properties of TiO_2 nanoparticles, such as photoreduction of CO_2 were investigated in terms of particle size. The results showed that the crystallite size plays an important role in nanocrystalline TiO_2-based photocatalysts. As the particle size decreased, higher yields of methanol and methane over the TiO_2 nanoparticles under the illumination of light were obtained. The optimum particle size corresponding to the highest yields of both products was 14 nm. For crystal sizes smaller than 14 nm the catalyst activity dropped probably due to the changes in optical and electronic properties of the nanometer crystal. The observed optimum particle size was a result of competing effects of specific surface area, charge–carrier dynamics and light absorption efficiency. The reduction of CO_2 by photocatalysts was one of the most promising methods, since CO_2 can be reduced to useful compounds by irradiating it with UV light. However, the efficiency of this method was relatively low and an increase of yield is necessary.

Acknowledgements

The financial support of the Czech Ministry of Education, Youth and Sports, research project MSM 6198910019 and AS CR Program Nanotechnology for Society (KAN 400720701) is gratefully acknowledged. Department of Condensed Matter Physics, Faculty of Mathematics and Physics, Charles University in Prague is gratefully acknowledged for XRD measurements and their evaluation by a modified FOX program.

References

[1] H. Yoneyama, Catal. Today 39 (1997) 169–175.
[2] H. Fujiwara, H. Hosokawa, K. Murakoshi, Y. Wada, S. Yanagida, J. Phys. Chem. B 101 (1997) 8270–8278.
[3] P. Johne, H. Kirsch, J. Photochem. Photobiol., A: Chem. 111 (1997) 223–228.
[4] B.-J. Liu, T. Torimoto, H. Yoneyama, J. Photochem. Photobiol., A: Chem. 113 (1998) 93–97.
[5] K. Sayama, H. Arakawa, J. Phys. Chem. 97 (1993) 531–533.
[6] Y. Kohno, T. Tanaka, T. Funabiki, S. Yoshida, Chem. Commun. 9 (1997) 841–842.
[7] Y. Kohno, T. Tanaka, T. Funabiki, S. Yoshida, J. Chem. Soc., Faraday Trans. 94 (1998) 1875–1880.
[8] Y. Kohno, T. Tanaka, T. Funabiki, S. Yoshida, Phys. Chem. Chem. Phys. 2 (2000) 2635–2639.
[9] Y. Kohno, T. Tanaka, T. Funabiki, S. Yoshida, Phys. Chem. Chem. Phys. 2 (2000) 5302–5307.
[10] S. Yoshida, Y. Kohno, Catal. Surv. Jap. 4 (2001) 107–114.
[11] Y. Kohno, H. Ishikawa, T. Tanaka, T. Funabiki, S. Yoshida, Phys. Chem. Chem. Phys. 3 (2001) 1108–1113.
[12] K. Teremura, T. Tanaka, H. Ishikawa, Y. Kohno, T. Funabiki, J. Phys. Chem. B 108 (2004) 346–354.
[13] N. Gokon, N. Hasegawa, H. Kaneko, H. Aoki, Y. Tamaura, M. Kitamura, Sol. Energy Mater. Sol. Cells 80 (2003) 335–341.
[14] B. Aurijan-Blajeni, M. Halman, J. Manassen, Sol. Energy 25 (1980) 165–170.
[15] W.K. Wong, M.A. Malati, Sol. Energy 36 (1986) 163–168.
[16] K. Hirano, K. Inoue, T. Yardu, J. Photochem. Photobiol., A: Chem. 64 (1992) 255–258.
[17] K. Adachi, K. Ohta, M. Mizuno, Sol. Energy 53 (1994) 187–190.
[18] M. Anpo, H. Yamashita, Y. Ichihashi, S. Ehara, J. Electroanal. Chem. 396 (1995) 21–26.
[19] H. Yamashita, A. Shiga, S. Kawasaki, Y. Ichihashi, S. Ehara, M. Anpo, Energy Convers. 36 (1995) 617–620.
[20] F. Saladin, L. Forss, I. Kamber, J. Chem. Soc., Chem. Commun. 5 (1995) 533–534.
[21] T. Mizuno, K. Adachi, K. Ohta, A. Saji, J. Photochem. Photobiol., A: Chem. 98 (1996) 87–90.
[22] M. Anpo, H. Yamashita, Y. Ichihashi, Y. Fuji, M. Honda, J. Phys. Chem. B 101 (1997) 2632–2636.
[23] S. Kaneco, H. Kurimoto, K. Ohta, T. Mizuno, A. Saji, J. Photochem. Photobiol., A: Chem. 109 (1997) 59–63.
[24] B.-J. Liu, T. Torimoto, H. Matsumoto, H. Yoneyama, J. Photochem. Photobiol., A: Chem. 108 (1997) 187–192.
[25] S. Kaneco, Y. Shimizu, K. Ohta, T. Mizuno, J. Photochem. Photobiol., A: Chem. 115 (1998) 223–226.
[26] B.-J. Liu, T. Torimoto, H. Yoneyama, J. Photochem. Photobiol., A: Chem. 115 (1998) 227–230.
[27] H. Yamashita, Y. Fijuu, Y. Ichihashi, S.G. Zhang, K. Ikeue, D.R. Park, K. Koyano, T. Tatsumi, M. Anpo, Catal. Today 45 (1998) 221–227.
[28] M. Subrahmanyam, S. Kaneco, N. Alonso-Vante, Appl. Catal., B: Environ. 23 (1999) 169–174.
[29] K. Kaneco, H. Kurimoto, Y. Shimizu, K. Ohta, T. Mizuno, Energy 24 (1999) 21–31.
[30] Y. Kohno, H. Hayashi, S. Takenaka, T. Tanaka, T. Funabiki, S. Yoshida, J. Photochem. Photobiol., A: Chem. 126 (1999) 117–124.
[31] I.-H. Tseng, W.-C. Cheng, J.C.S. Wu, Appl. Catal., B: Environ. 37 (2002) 37–48.
[32] I.-H. Tseng, J.C.S. Wu, H.-Y. Chou, J. Catal. 221 (2004) 432–440.

[33] G.R. Dey, A.D. Belapurkar, K. Kishore, J. Photochem. Photobiol., A: Chem. 163 (2004) 503–508.
[34] J.C.S. Wu, H.-M. Lin, C.-L. Lai, Appl. Catal., A: Gen. 296 (2005) 194–200.
[35] Slamet, H.W. Nasution, E. Purnama, S. Kosela, J. Gunlazuardi, Catal. Commun. 6 (2005) 313–319.
[36] N. Sasirekha, S.J.S. Basha, K. Shanthi, Appl. Catal., B: Environ. 62 (2006) 169–180.
[37] S.S. Tan, L. Zou, E. Hu, Catal. Today 115 (2006) 269–273.
[38] S.S. Tan, L. Zou, E. Hu, Sci. Tech. Adv. Mater. 8 (2007) 89–92.
[39] X.-H. Xia, Z.-J. Jia, Y. Yu, Y. Liang, Z. Wang, L.-L. Ma, Carbon 45 (2007) 717–721.
[40] S. Liu, Z. Zhao, Z. Wang, Photochem. Photobiol. Sci. 6 (2007) 695–700.
[41] C.-C. Lo, C.-H. Hung, C.-S. Yuan, J.-F. Wu, Sol. Eng. Mater. Sol. Cells 91 (2007) 1765–1774.
[42] V.N. Parmon, K.I. Zamareav, in: N. Serpone, E. Pelizzeti (Eds.), Photocatalysis: Fundamentals and Applications, John Wiley & Sons Ltd., USA, 1989 (Chapter 17).
[43] M.A. Fox, M.T. Dulay, Chem. Rev. 93 (1993) 341–357.
[44] Z. Zhang, C.-C. Wang, R. Zakaria, J.Y. Ying, J. Phys. Chem. 102 (1998) 10871–10878.
[45] N. Xu, Z. Shi, Y. Fan, J. Dong, J. Shi, M.Z.-C. Hu, Ind. Eng. Chem. Res. 38 (1999) 373–379.
[46] H.D. Jang, S.-K. Kim, S.-J. Kim, J. Nanopart. Res. 3 (2001) 141–147.
[47] A.J. Maira, K.L. Yeung, C.Y. Lee, P.L. Yue, C.K. Chan, J. Catal. 192 (2000) 185–196.
[48] W.C. Hao, S.K. Zheng, C. Wang, T.M. Wang, J. Mater. Sci. Lett. 21 (2002) 1627–1629.
[49] C.B. Almquist, P. Biswas, J. Catal. 212 (2002) 145–156.
[50] I.P. Muchlenov, J.I. Dobkinová, V.I. Derjužkinová, V.I., et al. Technologie katalyzátorů. SNTL Praha, 1985.
[51] H. Lin, C.P. Huang, W. Li, C. Ni, S.I. Shah, Y.-H. Tseng, Appl. Catal., B: Environ. 68 (2006) 1–11.
[52] J. Krýsa, M. Keppert, J. Jirkovský, V. Štengl, J. Šubrt, Mater. Chem. Phys. 86 (2004) 333–339.
[53] H. Krýsová, J. Krýsa, J. Jirkovský, G. Mailhot, M. Bolte, Appl. Catal., B: Environ. 40 (2003) 1–12.
[54] L. Brus, J. Phys. Chem. 90 (1986) 2555–2560.
[55] Z. Matěj, L. Nichtová, R. Kužel, Mater. Struct. 15 (2008) 46–49.
[56] http://objcryst.sourceforge.net/Fox/FoxWiki.
[57] G. Burgeth, H. Kisch, Coord. Chem. Rev. 230 (2002) 41–47.
[58] E.L. Simmons, Appl. Opt. 14 (1975) 1380–1386.
[59] G.F.A. Kortum, Reflectance Spectroscopy: Principles, Methods, Applications, New York, 1969.
[60] N.S. Lewis, M.L. Rosenbluth, in: N. Serpone, E. Pelizzetti (Eds.), Photocatalysis. Fundamentals and Applications, Wiley, New York, 1989, p. 99.
[61] M. Grätzel, in: N. Serpone, E. Pelizzetti (Eds.), Photocatalysis. Fundamentals and Applications, Wiley, New York, 1989, p. 123.
[62] M. Čeppan, M. Mikula, R. Fiala, V. Brezová, A. Blažková, J. Panák. Chem. Pap. 51 (1997), 193–X.
[63] R.B. Draper, M.A. Fox, Langmuir 6 (1990), 1396–X.
[64] NIOSH Manual of Analytical Method (NMAM), Fourth Edition, 8/15/94. Formaldehyde: Method 3500, Issue 2, 1994, pp. 2–5.
[65] L. Brus, J. Chem. Phys. 80 (1984) 4403–4409.
[66] A. Patsoura, D.I. Kondarides, X.E. Verykios, Catal. Today 124 (2007) 94–102.
[67] D.I. Kondarides, V.M. Daskalaki, A. Patsoura, X.E. Verykios, Catal. Lett. 122 (2008) 26–32.
[68] M. Horn, C.F. Schwerdtfeger, E.P. Meagher, Zeits. Kristallogr. 136 (1972) 273–281.
[69] R.K. Wahi, W.W. Yu, Y. Liu, M.L. Mejia, J.C. Falkner, W. Nolte, V.L. Colvin, J. Mol. Catal., A: Chem. 242 (2005) 45–56.
[70] M.A. Grela, A.J. Colussi, J. Phys. Chem. 100 (1996) 18214–18221.